Journal of Medicinal Chemistry

pubs.acs.org/jmc Article

Discovery of Dihydro-1,4-Benzoxazine Carboxamides as Potent and Highly Selective Inhibitors of Sirtuin-1

Martin Spinck,[‖] Matthias Bischoff,[‖] Philipp Lampe, Franz-Josef Meyer-Almes, Sonja Sievers, and Heinz Neumann*

Cite This: *J. Med. Chem.* 2021, 64, 5838−5849 Read Online

ACCESS | Metrics & More | Article Recommendations | Supporting Information

ABSTRACT: Sirtuins are signaling hubs orchestrating the cellular response to various stressors with roles in all major civilization diseases. Sirtuins remove acyl groups from lysine residues of proteins, thereby controlling their activity, turnover, and localization. The seven human sirtuins, SirT1−7, are closely related in structure, hindering the development of specific inhibitors. Screening 170,000 compounds, we identify and optimize SirT1-specific benzoxazine inhibitors, Sosbo, which rival the efficiency and surpass the selectivity of selisistat (EX527). The compounds inhibit the deacetylation of p53 in cultured cells, demonstrating their ability to permeate biological membranes. Kinetic analysis of inhibition and docking studies reveal that the inhibitors bind to a complex of SirT1 and nicotinamide adenine dinucleotide, similar to selisistat. These new SirT1 inhibitors are valuable alternatives to selisistat in biochemical and cell biological studies. Their greater selectivity may allow the development of better targeted drugs to combat SirT1 activity in diseases such as cancer, Huntington's chorea, or anorexia.

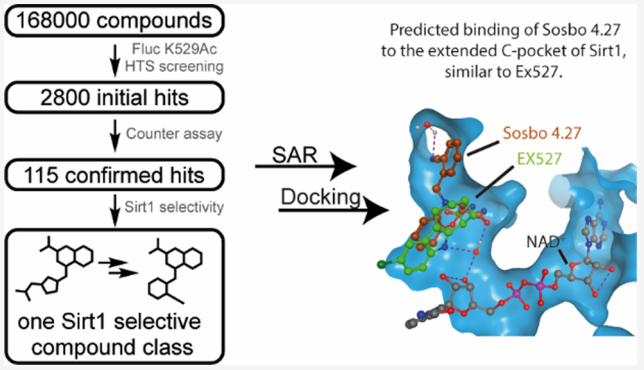

INTRODUCTION

Sirtuins are nicotinamide adenine dinucleotide (NAD^+)-dependent lysine deacylases conserved in all three domains of life. Their biological importance is illustrated by the multitude of physiological processes they contribute to. Accordingly, there is a role for a sirtuin in nearly every prominent disease, including neurodegeneration, diabetes, arteriosclerosis, cancer, and aging.[1] Drugs to modulate sirtuin activity, both positively and negatively, are highly sought after.[2] Particularly, SirT1, whose activity has been positively correlated with longevity,[3] has received much attention in the past two decades. SirT1 substrates encompass, i.a., histones[4] and transcription factors such as PGC1-α,[5,6] FOXOs,[7,8] and p53.[9,10] By controlling their acetylation status, SirT1 acts as a metabolic stress sensor that integrates fluctuations in intracellular NAD^+ concentrations[11−13] and signaling from upstream kinases, for example, protein kinase A,[14] into an adequate response.

Deacetylation of lysine residues by sirtuins involves the stoichiometric cleavage of NAD^+ into nicotinamide (NAM) and *O*-acetyl-ADP-ribose (OAADPR).[15] NAD^+ is bound to a canonical Rossman fold domain, and the NAM moiety is accommodated in the C-pocket upon binding of the peptide substrate.[16] Cleavage of NAM leads to the formation of a carbenium ion, which subsequently attacks the carbonyl-oxygen of the acetyl group. The intermediate undergoes an intramolecular rearrangement and is eventually hydrolyzed, releasing the deacetylated peptide and OAADPR.[17] The cleavage product NAM can rebind the enzyme and regenerate NAD^+ creating a negative feedback mechanism.[18]

Sirtuin-activating compounds promise to improve healthy aging[2] because increased levels of sirtuin activity have been correlated with an increase in the lifespan of various organisms.[19−21] Inhibitors of SirT2 are being explored for their benefits in the treatment of neurodegenerative disorders, whereas SirT1 inhibitors may find applications in the treatment of cancer, Huntington's disease, or anorexia.[22,23]

The best in class inhibitor for SirT1, selisistat, is currently tested in clinical trials for the treatment of Huntington's chorea.[24] Selisistat inhibits SirT1 with two-digit nanomolar IC_{50} and is approximately 100-fold less potent against closely related sirtuins SirT2 and SirT3.[22]

Nevertheless, selisistat is routinely used in cells at micromolar concentration to inhibit SirT1, a level sufficient to affect other sirtuins.[25,26] Alternative scaffolds for the design of even

Received: January 6, 2021
Published: April 20, 2021

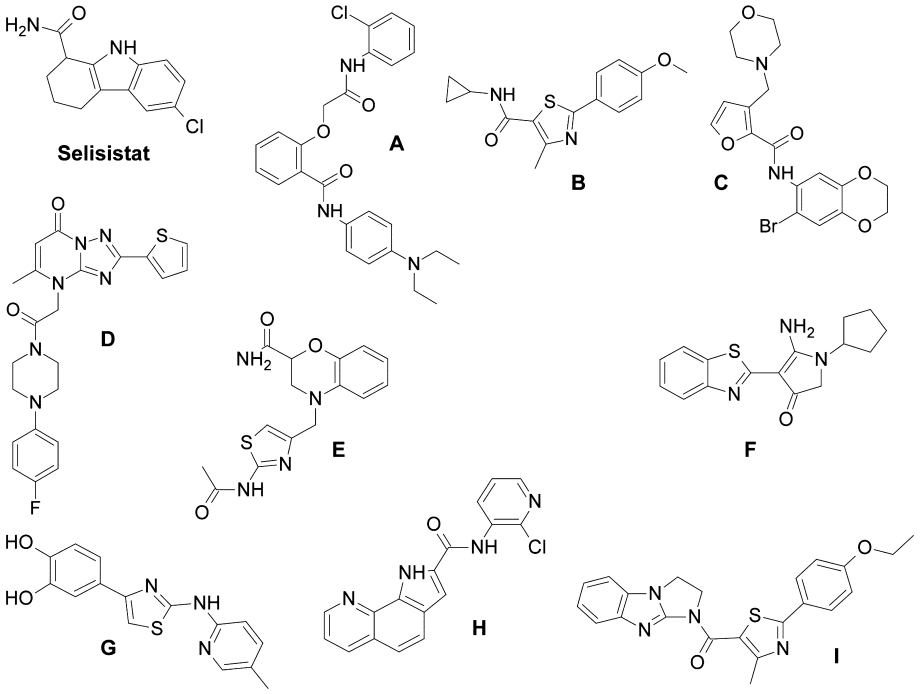

Figure 1. Structures of compounds.

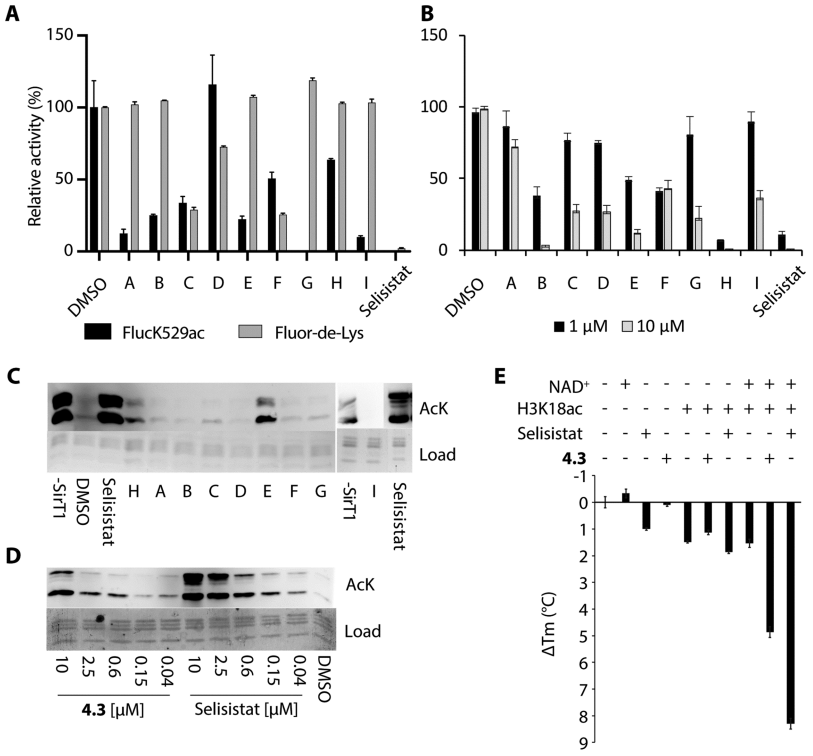

Figure 2. Inhibition of SirT1 by initial hits. (A) Inhibition of SirT1 by nine initial hit compounds (1 μM) and selisistat (1 μM) measured with FLucK529ac and Fluor-de-Lys (B) SirT-Glo assays with 1 and 10 μM compounds. (C) In vitro deacetylation assay of acetylated histone proteins (0.25 mg/mL) by purified SirT1 (100 nM) in the presence of indicated compounds (10 μM) or DMSO. Compound I was tested in a separate experiment. (D) Dose-dependent inhibition of histone deacetylation by **4.3** (E) and selisistat. Uncropped images of the blots in Figure S1. (E) Thermal denaturation of SirT1 (SYPRO orange, T_m: 41.5 °C, and 1 mg/mL) bound to different combinations of NAD^+ (1 mM), H3K18ac histone peptide (1 mM), and selisistat or **4.3** (0.1 mM each). Error bars represent the standard deviation of triplicate measurements.

more specific SirT1 inhibitors may therefore become valuable as tools in basic research and for the development of improved drugs.[27] Here, we performed a high-throughput screening (HTS) for inhibitors of recombinant human SirT1 using firefly luciferase acetylated at active site lysine K529 (FLucK529ac) as the substrate.[28] Thereby, we identified and optimized a promising new class of highly potent and specific SirT1 inhibitors with a benzoxazine scaffold. Because of their

https://doi.org/10.1021/acs.jmedchem.1c00017
J. Med. Chem. 2021, 64, 5838−5849

Scheme 1[a]

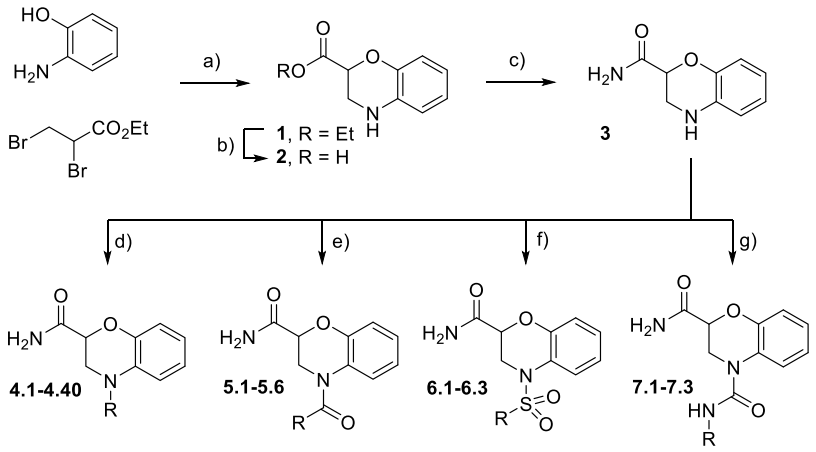

[a](a) K_2CO_3, acetone, 75 °C, 22 h, and 67%; (b) LiOH, H_2O/tetrahydrofuran (THF), RT, 1 h, and 93%; (c) NH_4OH, EtOH, 80 °C, 20 h, and 75%; (d) RX, K_2CO_3, NaI, acetone, 65 °C or RCHO, $NaBH(OAc)_3$, DCM, and RT; (e) RCOCl, NEt_3, DCM, and 0 °C to RT; (f) RSO_2Cl, NEt_3, dioxane, and 100 °C; (g) RNCO, NEt_3, DCM, and 0 °C to RT.

pronounced selectivity for SirT1 over other sirtuins, we decided to name this new inhibitor class *Sosbo* (for "**s**irtuin **o**ne **s**elective **b**enz**o**xazine").

RESULTS AND DISCUSSION

Identification of a New Class of SirT1 Inhibitors. Using a recently developed sirtuin activity assay based on FLucK529ac,[28] we screened a library of approximately 170,000 compounds for inhibitors of SirT1. From the primary screen, 2800 compounds were retested for SirT1 inhibition with FLucK529ac and for direct inhibition of luciferase, which narrowed down the list of candidate compounds to 135. Pan-assay interference compound (PAINS) filtering[29] and testing against redox-cycling behavior[30] further reduced the number to 115 initial hits. These were subsequently tested for their selectivity toward SirT1 compared to SirT2 and SirT3 (Table S1).

Nine initial hits were selected for further analysis based on their potency and selectivity (Figure 1). With an IC_{50} value of 620 nM, dihydro-1,4-benzoxazine **4.3** (E) showed remarkable potency to inhibit SirT1, while SirT2 and SirT3 were not affected up to 60 μM. This inhibitory activity is only 13 times lower and more selective than the gold standard of SirT1 inhibitors, selisistat,[22] which we used as a reference compound. Surprisingly, we did not detect any inhibitory activity of **4.3** using the Fluor-de-Lys assay (Figure 2A). We therefore used an orthogonal SirT-Glo assay (Promega) to test the selected set of compounds (Figure 2B and Table S2). This assay depends on the release of luciferin from the C-terminus of a peptide upon deacetylation. Again we observed SirT1 inhibition only by a subset of the compounds, suggesting that inhibition by most of these compounds is substrate-dependent.

To test the SirT1 inhibition on a physiological substrate, we performed deacetylation reactions with isolated human histones (Figure 2C). Only selisistat and **4.3** were able to prevent deacetylation in a dose-dependent manner (Figure 2D). Thermal shift assays showed that the interaction of **4.3** with SirT1 depends on the presence of a substrate peptide and is enhanced by NAD^+ (Figure 2E). Selisistat stabilized SirT1 against heat denaturation similar to **4.3**, indicating that they might act by the same mechanism.

Structure–Activity Relationship (SAR) Analysis of Benzoxazine Compounds. We decided to focus our further investigation and hit optimization on the benzoxazine scaffold of **4.3**. The general synthesis of the dihydro-1,4-benzoxazine scaffold is outlined in Scheme 1.[31,32] 2-Aminophenol is alkylated with ethyl 2,3-dibromopropanoate in the presence of K_2CO_3 as a base in 67% yield. The ester **1** is either hydrolyzed to the carboxylic acid **2** using LiOH or directly transformed to the amide **3** by treatment with NH_4OH in ethanol in 75% yield.

Amide **3** serves as a platform for the introduction of various substituents at the 4 position. Reaction with alkyl halides or reductive amination with aldehydes led to amines **4.1–4.40**, reaction with acid chlorides led to amides **5.1–5.6**, reaction with sulfonyl chlorides led to sulfonamides **6.1–6.3**, and reaction with isocyanates led to ureas **7.1–7.3** (Table 1). First of all, we resynthesized the hit compound **4.3** by alkylation of **3** with *tert*-butyl (4-(chloromethyl)thiazol-2-yl)carbamate, Boc-deprotection, and acetylation. The activity of compound **4.3** could be confirmed, whereas the aminothiazole **4.2** and the *N*-Boc aminothiazole **4.1** showed lower activities. Subsequently, we replaced the thiazole moiety by various substituted aromatic, as well as heteroaromatic rings. The presence of an aromatic ring proved to be essential for activity, as hydrogen (**3**), methyl (**4.4**), propargyl (**4.17**), or *tert*-butyl acetate (**4.20**) in the 4 position showed no activity.

Electron-withdrawing functional groups, for example, nitro (**4.21** and **4.22**) or cyano (**4.27** and **4.28**) in meta- and ortho-positions, decreased the IC_{50} to 150–430 nM, whereas increased bulk (e.g., **4.14**, **4.18**, **4.19**, and **4.38**) and electron-donating groups (e.g., **4.23** and **4.29**) reduced the potency of the compounds. *N*-acetyl substitution in ortho-, meta-, or para-positions (**4.24**, **4.25**, and **4.26**) did not reach the activity of *N*-acetyl thiazole **4.3.** Halogen substituents such as chloride, bromide, and iodide or a methyl ester in the ortho-position (**4.32**, **4.33**, **4.34**, and **4.39**) showed all activity in the submicromolar region. Interestingly, the introduction of two trifluoromethyl groups turned **4.9** into a potent and quite specific inhibitor of SirT2. The linkage between the benzoxazine core and the aromatic substituent was also very important. Changing the functional group from an amine to an amide (**5.1–5.6**), a sulfonamide (**6.1–6.3**), or a urea (**7.1–**

https://doi.org/10.1021/acs.jmedchem.1c00017
J. Med. Chem. 2021, 64, 5838–5849

Table 1. SAR Investigation of the Substituents R^1 and R^2 with IC_{50} Values Given as Arithmetic Means of Four Technical Replicates

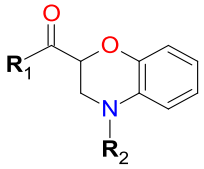

Compound	R^1	R^2	Sirtuin 1 IC_{50} [μM]	Sirtuin 2 IC_{50} [μM]	Sirtuin 3 IC_{50} [μM]
Selisistat *	-	-	0.048	0.50	6.4
1	OEt	H	> 60	> 60	> 60
2	OH	H	> 60	> 60	> 60
3	NH_2	H	> 60	> 60	> 60
4.1	NH_2	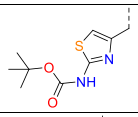	5.63	> 60	> 60
4.2	NH_2		1.48	> 60	> 60
4.3 *	NH_2	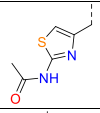	0.62	> 60	> 60
4.4	NH_2		> 60	> 60	> 60
4.5	NH_2		8.54	> 60	> 60
4.6	NH_2	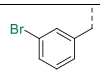	1.27	1.76	> 60
4.7	NH_2	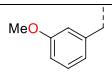	2.13	15.4	> 60
4.8	NH_2	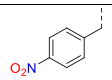	1.06	34.7	> 60
4.9	NH_2	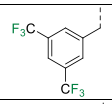	6.04	0.52	> 60
4.10	NH_2	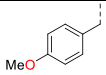	1.45	31.8	> 60
4.11	NH_2	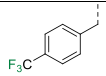	28.5	22.8	> 60
4.12	NH_2		0.82	12.3	> 60
4.13	NH_2	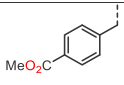	3.45	> 60	> 60
4.14	NH_2	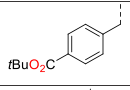	20.1	42.0	> 60
4.15	NH_2		2.10	> 60	> 60
4.16	NH_2		4.70	58.0	> 60
4.17	NH_2		> 60	> 60	> 60
4.18	NH_2	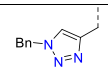	8.05	41.9	> 60
4.19	NH_2		14.1	32.6	> 60
4.20	NH_2		> 60	> 60	> 60
4.21	NH_2	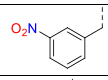	0.23	4.19	> 60
4.22	NH_2	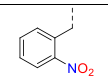	0.15	10.6	> 60
4.23	NH_2	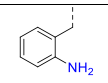	4.91	36.1	> 60
4.24	NH_2	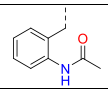	31.6	> 60	> 60
4.25	NH_2	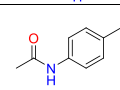	10.4	> 60	> 60
4.26	NH_2	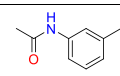	2.40	> 60	> 60
4.27 *	NH_2		0.22	37.7	> 60
4.27 * ent-1	NH_2		47.3	47.3	> 60
4.27 * ent-2	NH_2		0.11	34.0	> 60
4.28	NH_2	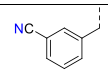	0.43	11.2	> 60
4.29	NH_2	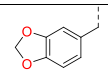	1.90	26.0	> 60
4.30	NH_2	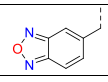	0.60	12.9	> 60

https://doi.org/10.1021/acs.jmedchem.1c00017
J. Med. Chem. 2021, 64, 5838−5849

Table 1. continued

Compound	R^1	R^2	Sirtuin 1 IC_{50} [μM]	Sirtuin 2 IC_{50} [μM]	Sirtuin 3 IC_{50} [μM]
Selisistat *	-	-	0.048	0.50	6.4
4.31	NH_2		1.77	35.4	> 60
4.32	NH_2		0.67	33.6	> 60
4.33	NH_2		0.56	16.6	> 60
4.34	NH_2		0.47	> 60	> 60
4.35	NH_2		0.97	25.0	> 60
4.36	NH_2		2.49	22.2	> 60
4.37	NH_2		37.4	> 60	> 60
4.38	NH_2	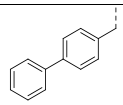	> 60	> 60	> 60
4.39	NH_2	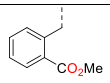	0.49	> 60	> 60
4.40	NH_2	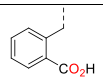	13.9	> 60	> 60
5.1	NH_2		> 60	> 60	> 60
5.2	NH_2		> 60	> 60	> 60
5.3	NH_2		> 60	> 60	> 60
5.4	NH_2		> 60	> 60	> 60
5.5	NH_2	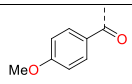	> 60	> 60	47.8
5.6	NH_2	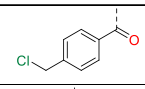	48.8	> 60	> 60
6.1	NH_2		> 60	> 60	> 60
6.2	NH_2	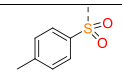	> 60	> 60	> 60
6.3	NH_2	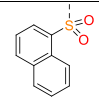	> 60	> 60	> 60
7.1	NH_2	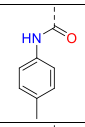	> 60	45.6	> 60
7.2	NH_2	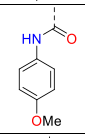	> 60	> 60	> 60
7.3	NH_2	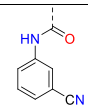	49.0	> 60	> 60
8	OEt		> 60	> 60	> 60
9	OH		> 60	> 60	> 60
10.1	NHMe		> 60	> 60	> 60
10.2	NMe_2		> 60	> 60	> 60
10.3			> 60	> 60	> 60

[a]Measured separately using an inhibitor concentration range of 0.003−60 μM.

Scheme 2[a]

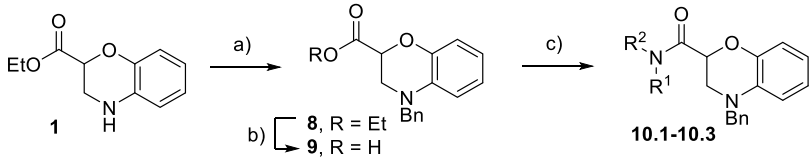

[a](a) BnBr, K_2CO_3, NaI, acetone, 65 °C, 18 h, and 76%; (b) LiOH, H_2O/THF, RT, 18 h, and 94%; and (c) NR_1R_2, HATU, DIPEA, DMF, and RT.

7.3) completely abolished SirT1 inhibition. Eventually, we probed the SAR of the carboxamide group in the 2-position of the benzoxazine (Scheme 2).

To this end, ester **1** was *N*-alkylated with benzyl bromide and K_2CO_3 as a base in 76% yield. The ester was hydrolyzed using LiOH, and the resulting carboxylic acid was coupled with methylamine, dimethylamine, and piperidine to afford the amides **10.1**, **10.2**, and **10.3**. Neither ester **8** or carboxylic acid **9** nor any of the secondary or tertiary amides showed any activity, highlighting the importance of a primary amide group (Table 1).

https://doi.org/10.1021/acs.jmedchem.1c00017
J. Med. Chem. 2021, 64, 5838−5849

Finally, we were interested in the different activities of the enantiomers of the dihydro-1,4-benzoxazines. Therefore, we chose compound **4.27** as the most active and selective one. The enantiomers of **4.27** were separated on a chiral stationary phase, and their activity against SirT1, SirT2, and SirT3 was tested. Enantiomer-2 of **4.27** inhibited SirT1 with an IC_{50} value of 110 nM, about half the activity of the racemate, whereas the IC_{50} of enantiomer-1 of **4.27** was approximately 400-fold higher. Neither of the enantiomers showed significant activity against the other sirtuins up to 60 μM.

Benzoxazines Inhibit SirT1 in Cultured Human Cells. SirT1 counteracts activation of p53 by reverting acetylation of Lys-382.[9,10] The acetylation stabilizes p53 against ubiquitin-dependent proteasomal degradation in vivo. Inhibition of SirT1 by selisistat blocks deacetylation of this residue and leads to increased p53 levels in the presence of genotoxic compounds such as etoposide.[33] In contrast, the pan-specific sirtuin inhibitor NAM does not enhance p53 acetylation in cultured mammalian cells.[33] We treated MDA-MB-231 cells, a human breast adenocarcinoma cell line with intact p53, with etoposide and increasing concentrations of selisistat, **4.22**, or **4.27** (Figure 3). All three compounds induced a strong increase in the level of p53 K382ac, indicating that the benzoxazines are cell permeable and active in vivo.

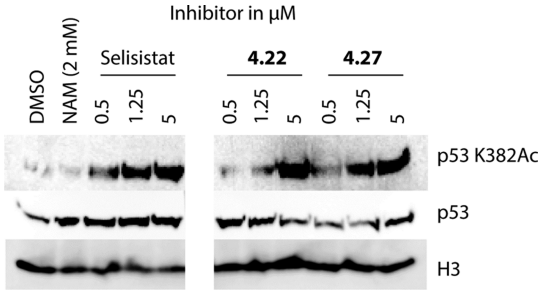

Figure 3. Benzoxazines inhibit SirT1 in vivo. Etoposide (50 μM for 20 h) preincubated MDA-MB-231 cells were treated for 3 h with DMSO, NAM (2 mM), selisistat, **4.22**, or **4.27** (0.5, 1.25, or 5 μM). Acetylation of p53 K382 was subsequently measured by western blotting using modification-specific antibodies (biological replicates of the experiment are shown in Figure S2).

Benzoxazines Are Uncompetitive Inhibitors of SirT1. Selisistat is an uncompetitive inhibitor with respect to NAD^+.[22,34] The partial structural similarity of the new SirT1 inhibitors to selisistat prompted us to analyze their mode of inhibition. Therefore, we measured apparent V_{max} and K_M values for selisistat, **4.22**, and **4.27** in dependence of the NAD^+ concentration (Figure 4A). In all three cases, we observed a reduction of V_{max} and K_M characteristic of uncompetitive inhibition. Hence, selisistat and benzoxazines may share a common mechanism of inhibition. Next, we tested binding of the inhibitors to SirT1−3 in dependence of substrates by thermal shift assays (Figure 4B). None of the inhibitors showed any stabilization of SirT2 or SirT3 at a concentration of 90 μM, demonstrating their pronounced specificity. Selisistat stabilized SirT1 only in the presence of NAD^+, in line with it being part of the binding pocket of the inhibitor.[35] The additional presence of substrate peptide (H3K18ac) further stabilized the complex, suggesting that SirT1 is able to simultaneously bind selisistat and both substrates. Compounds **4.3** and **4.27** showed the same pattern of SirT1 stabilization, indicating that they bind similar to selisistat to the extended C-pocket.[34]

Molecular Docking of 3,4-Dihydro-2H-1,4-Benzoxazines into SirT1. At first, the docking routine was validated by redocking of the selisistat analogue into the crystal structure of its complex with SirT1 (PDB-ID 4I5I).[35] The docked and crystallized poses of the ligand within the binding pocket of SirT1 show excellent overlap with a root mean square deviation (RMSD) of 0.408 Å (Figure S3). Thus, the applied docking procedure with binding site definition including structural water molecules and cofactor NAD^+ is suitable for providing reliable docking poses for SirT1-inhibitors. To rationalize the inhibitory activity of 3,4-dihydro-2H-1,4-benzoxazines, the structures were docked into the crystal structure of SirT1.

When looking at the binding mode of the selisistat analogue and the cofactor NAD^+ within the active site of SirT1, it becomes obvious that several structural water molecules play important roles for binding of the selisistat analogue to amino acids of the binding pocket and cofactor NAD^+ (Figure 5). Therefore, the usage of NAD^+ and structural water molecules as the integral part of the binding pocket appears perfectly justified. Docking of 21 benzoxazine analogues shows similar trends for the GBVI/WSA dG docking score of MOE and pIC_{50}-values of the compounds with a Pearson correlation coefficient of $r = -0.57$ (Table S3 and Figure S4). In addition, the docking poses of the benzoxazine core of most potent compounds (IC_{50}-values <5 μM) show excellent overlap, while larger variations are observed for the substituents in the 4-position (Figure 5B and Figure S5).

The benzoxazine core snuggles perfectly into the binding pocket of SirT1 showing considerable overlap with the selisistat analogue in the crystal structure of SirT1 (Figure 5A). Moreover, the selisistat analogue, as well as the 3,4-dihydro-2H-1,4-benzoxazines, binds very similarly to SirT1 by direct hydrogen bonds between an amide nitrogen and the side chain carboxyl group of D348, as well as between I347 and different ligand atoms and indirectly by hydrogen bonds through structural water molecule 702 to the backbone carbonyl oxygens of A262 and P271 (Figure 5A and Figure S6).

In addition, selisistat, as well as the benzoxazine core, forms hydrogen bonds to another structural water 717, which is connected with two different oxygen atoms of cofactor NAD^+ by further hydrogen bonds (Figure 5A). Because of the perfect and reproducible steric fit of the benzoxazine core into the binding pocket, the positions of both bridging water molecules, 702 and 717, are also highly conserved. In addition and very similar to the selisistat analogue, the benzoxazine core shows Pi-Pi interactions with F273 and F297 (Figure S6).

In contrast to the benzoxazine core, the substituents in the 4-position show a considerable shift. However, it is noteworthy that many analogues are still able to form hydrogen bonds to structural water molecule 732, although with larger positional variations (Figure 5B and Figure S5). This water molecule is also fixed to SirT1 by hydrogen bonds to Y317 and Q320. The substituents of the benzoxazine analogues are accommodated in the upper region of the binding pocket of SirT1 close to the entrance (Figure S7).

Interestingly, the access to the active site is rather restricted because of a very narrow entrance area according to the crystal structure of SirT1[35] (PDB-ID 4I5I, Figure S7). Obviously, the adjacent region of the upper part of the binding pocket has to

https://doi.org/10.1021/acs.jmedchem.1c00017
J. Med. Chem. 2021, 64, 5838−5849

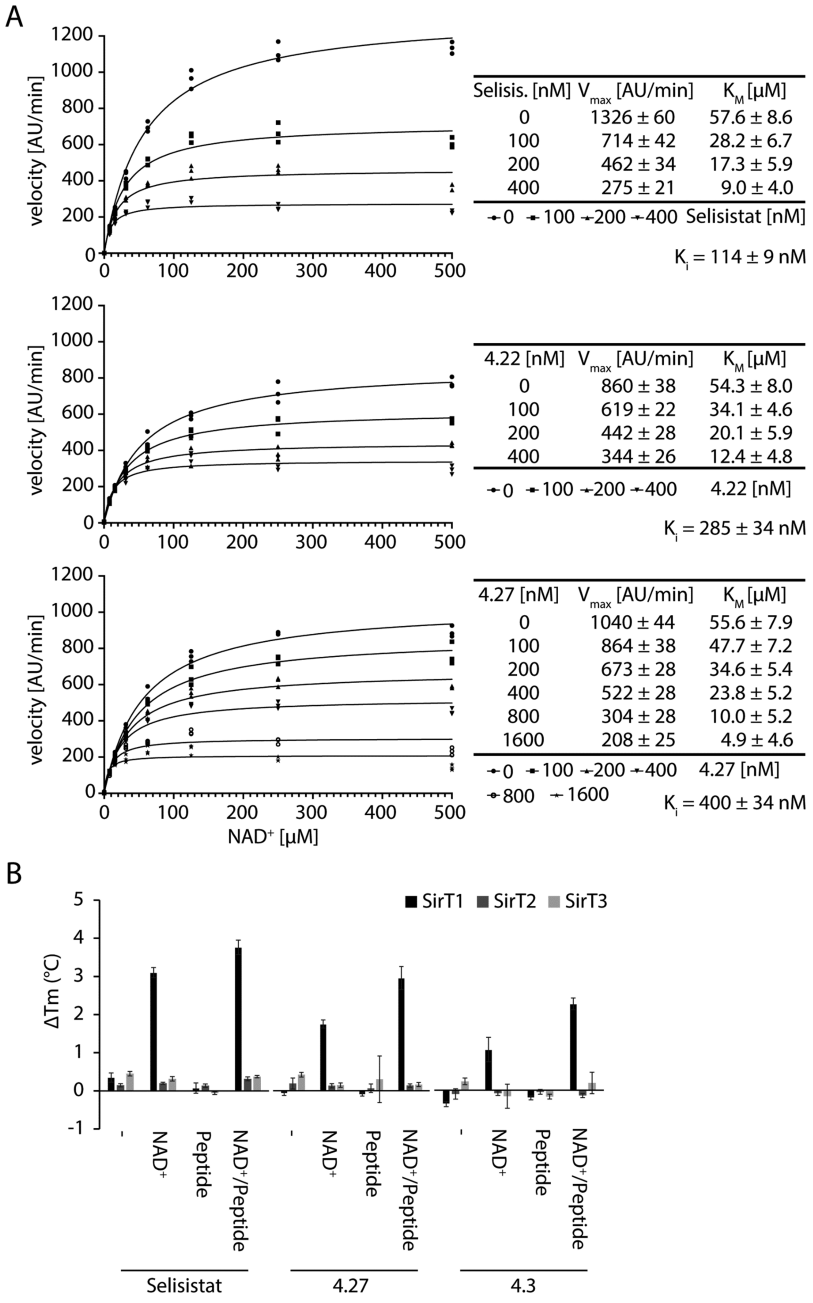

Figure 4. Kinetic characterization of SirT1 inhibition by **4.22** and **4.27**. (A) Michaelis−Menten kinetics of selisistat, **4.22,** and **4.27** measured using the continuous FLucK529ac assay. K_M, K_i, V_{max}, and error range were determined for different inhibitor concentrations by fitting the data using the Michaelis−Menten model of GraphPad Prism 8. (B) Thermal denaturation of SirT1−3 bound to different combinations of NAD^+, acetylated histone peptide (H3K18ac for SirT1/3 and H4K16ac for SirT2) and selisistat, **4.27**, or **4.3**.

be rather flexible to enable the access of compounds such as selisistat or **4.27**. This expected behavior is consistent with larger B-factors particularly in the loop between I316 and S324 and the docking poses of 3,4-dihydro-2H-1,4-benzoxazine analogues with a broader range of topologies for the substituents in the 4-position, as well as the pronounced adaptability of structural water 732, which is attached to Y317 and Q320 in the putative flexible loop.

Altogether, the 3,4-dihydro-2H-1,4-benzoxazines and selisistat show large structural overlap and very similar molecular interactions. The cofactor NAD^+ and three structural water molecules (702, 717, and 732), as well as Pi-Pi interactions with F273 and F297, are essential for the molecular recognition of 3,4-dihydro-2H-1,4-benzoxazine analogues.

Finally, we compared the binding properties of the two enantiomers of **4.27** (Figure S8). The docking score of the R-enantiomer (−6.7) is significantly poorer than that of the S-enantiomer (−7.8). Although the benzoxazine core of both enantiomers shows significant overlap, the constraints of the binding pocket and the different configurations at the chiral C-atom enforce a considerable distortion of the oxazine ring in the R-enantiomer of **4.27**. This results in the formation of only one hydrogen bond to D348 for the R-enantiomer of **4.27**, while the S-enantiomer shows three hydrogen bonds to D348 and structural water molecules 717 and 732. Therefore, we

https://doi.org/10.1021/acs.jmedchem.1c00017
J. Med. Chem. 2021, 64, 5838−5849

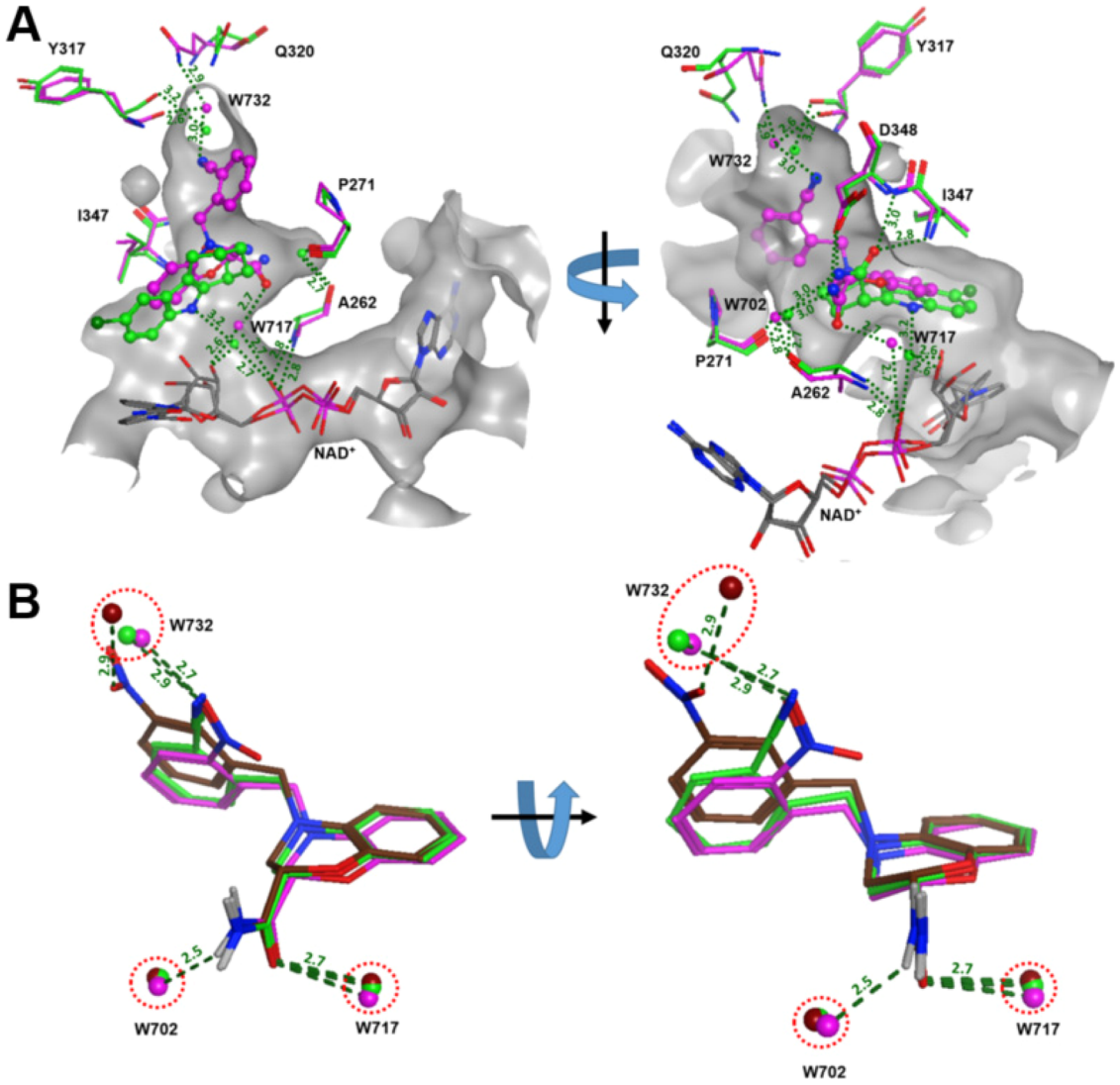

Figure 5. Molecular docking of 3,4-dihydro-2H-1,4-benzoxazines into SirT1. (A) Overlay of the crystallized selisistat analogue (green ball and stick) and docked **4.27** (magenta ball and stick) within the binding pocket of SirT1 (PDB-ID 4I5I). Amino acids that are important for the recognition of the ligand and cofactor are shown and colored (green: crystal structure and magenta: docked and energy minimized complex). The elongated lower active site pocket is occupied by cofactor NAD^+. The two slightly different conformations of NAD^+ and adjacent amino acids result from energy minimization of the docking result. Structural water molecules are displayed as solid beads and annotated according to the corresponding PDB data set. Hydrogen bonds are shown as dark green dotted lines. Additional hydrophobic interactions are not shown for the sake of clarity. (B) Overlay of docking poses of most potent SirT1 inhibitors. Best compounds, **4.21**, **4.22,** and **4.27**, and corresponding structural water molecules are colored in dark brown, magenta, and green, respectively. The positions of structural water molecules in different docking poses are highlighted by red dotted circles. Water molecules are shown as beads and numbered with a leading W. Distances in Ångström between heavy atoms of hydrogen bonds are indicated as dark green numbers.

suggest that **4.27** ent-2, which is the more potent SirT1 inhibitor, is the S-enantiomer.

CONCLUSIONS

Using a new lysine deacetylase assay based on FLucK529ac, we identified a new class of compounds with excellent inhibitory properties for SirT1. The traditional Fluor-de-Lys assay would not have identified the initial hit (Figure 2A), emphasizing the benefit of orthogonal assays in compound screening. The SAR analysis revealed critical functionalities of the inhibitor and allowed us to improve their activity.

Our initial studies with cultured human cells proved their ability to pass the plasma membrane and to act on cellular targets. At the same time, we observed no apparent toxicity at concentrations sufficient to inhibit deacetylation of p53. Hence, Sosbo inhibitors will be a valuable tool to investigate the cellular role of SirT1. This is important to identify potential side effects of selisistat.

The mode of SirT1 binding by Sosbo inhibitors is likely to be similar to that of selisistat. Both act as uncompetitive inhibitors that bind to the enzyme−substrate complex. The docking studies suggest that Sosbo compounds are extended C-site inhibitors.[34] Structural studies on the SirT1/Sosbo complex are essential for their further optimization.

EXPERIMENTAL SECTION

Plasmids and Strains. Strains and plasmids used in this study are listed in Table S4.

Expression and Purification of the SirT1, SirT2, and SirT3 Catalytic Domain. BL21(DE3) was transformed with the pBK-His_6-

https://doi.org/10.1021/acs.jmedchem.1c00017
J. Med. Chem. 2021, 64, 5838−5849

SirT2/3 (50 μg/mL kanamycin, kan) or pCDF-His$_6$-SirT1 (50 μg/mL spectinomycin, spec) plasmid. A 10 mL LB (50 μg/mL kan or spec) overnight culture was incubated at 37 °C with shaking 200 rpm. One liter of culture (LB, 50 μg/mL kan or spec) was inoculated with the overnight culture and grown at 37 °C and 200 rpm to an OD_{600} of 0.8 (SirT1) or 0.3 (SirT2/3). Expression was induced by addition of 0.5 mM IPTG (SirT1) or 0.2% arabinose (SirT2/3) and culture-shifted to 18 °C (SirT1) or 30 °C (SirT2/3). The cells were harvested by centrifugation, and the pellet was washed with PBS and stored at −20 °C. For purification, the cell pellet was thawed on ice and resuspended in sirtuin wash buffer (20 mM Tris pH 8, 200 mM NaCl, 20 mM imidazole, and 1 mM DTT) supplemented with 0.2 mM PMSF, lysozyme (0.5 mg/mL), and DNAse (∼1 mg). The digested cells were lysed by two passages through a pneumatic cell disintegrator. The lysate was cleared by centrifugation (20 min, 20.000 rpm, and 4 °C), and 500 μL Ni^{2+}-NTA resin was added to the supernatant. The suspension was agitated for 1 h (SirT1/3) or 24 h (SirT2) at 4 °C after which the beads were collected by passing the suspension over a plastic column with a frit. The beads were washed with 40 mL of sirtuin wash buffer, and the protein was eluted with 4 mL of sirtuin wash buffer supplemented with 200 mM imidazole. The buffer was exchanged for sirtuin gel filtration buffer (20 mM Tris pH 8, 50 mM NaCl, and 10 mM DTT) before the concentrated protein was applied to an HILoad 26/60 Superdex 200 size-exclusion chromatography column (GE healthcare) equilibrated with gel filtration buffer. By monitoring the UV absorption at 280 nm, fractions containing protein were identified and analyzed by sodium dodecyl sulfate polyacrylamide gel electrophoresis (SDS-PAGE). The pure fractions were concentrated, aliquoted, and flash-frozen in liquid nitrogen for storage at −80 °C.

FLucK529ac Lysine Deacetylase Assay. FLucK529ac was produced by genetic code expansion to install acetyllysine at the active site residue K529 of Firefly Luciferase as described previously.[28] Deacetylase activities were measured in continuous format. Briefly, the reaction mixture was prepared in triplicate in a 96-well plate each well containing 100 nM SirT1, diluted FLucK529ac (ca. 270 nM), and 100−1600 nM sirtuin inhibitor in a final volume of 40 μL sirtuin buffer 2 (25 mM Tris/HCl pH 8.0, 137 mM NaCl, 2.7 mM KCl, 1 mM $MgCl_2$, and 1 mM GSH). Fifty microliters of 2× luciferase buffer (40 mM tricine, 200 μM EDTA, 7.4 mM $MgSO_4$, 2 mM $NaHCO_3$, 34 mM DTT, 0.5 mM ATP, and 0.5 mM luciferin and pH 7.8) were added before the reaction was started by addition 10 μL of 10-fold concentrated NAD^+ (0−5000 μM). The reaction mixture was preincubated for 2 min at room temperature before the luminescence of each well was recorded over 30 min at room temperature. The KDAC activity was calculated from the slope of the linear reaction phase. The kinetic parameters and error ranges were retrieved by fitting the data using the GraphPad Prism 8 (v8.4.3) standard Michaelis−Menten function with the preset parameters.

HTS Format. Compounds were dispensed into dry white 1536-well plates (Corning 3729). Two microliters of a mixture of 30 nM Sirt1 and diluted firefly luciferase (ca. 90 nM; 1:3000) FLucK529ac in 25 mM Tris/HCl pH 8.0, 137 mM NaCl, 2.7 mM KCl, and 1 mM $MgCl_2$ were added and incubated for 15 min at RT. Two microliters of 2 mM NAD^+ were added to start the reaction. After 30 min, 4 μL of 2× luciferase buffer were added to detect luciferase activity. After 10 min, luminescence was read with an Envision reader (PerkinElmer).

Luciferase Counter-Assay. Compounds were dispensed into dry white 384-well plates (Corning 4513). Eight microliters of 0.5 nM firefly luciferase (Sigma, #L9506) in 25 mM Tris/HCl pH 8.0, 137 mM NaCl, 2.7 mM KCl, 1 mM GSH, 3 μM DTT, and 1 mM NAD^+ were added and incubated for 30 min at RT. Eight microliters of luciferin solution were added to start the reaction. After 30 min, luminescence was read with a Paradigm Spectramax reader.

IC_{50} Measurements. Compounds were dispensed with the highest assay concentration of 60 μM in 8 or 12 dilution steps as indicated and a factor of 3 into dry white 384-well plates (Corning 4513). Four microliters of either 30 nM SirT1 or 47 nM SirT2 or 103 nM SirT3 and diluted firefly luciferase FLucK529ac (ca. 90 nM; 1:3000) in sirtuin buffer containing 25 mM Tris/HCl pH 8.0, 137 NaCl, 2.7 mM KCl, 1 mM $MgCl_2$, and 1 mM GSH were added and incubated for 15 min at RT. Four microliters of 2 mM NAD^+ in sirtuin buffer were added to start the reaction. After 30 min at RT, 8 μL of 2x luciferase buffer were added to detect luciferase activity. After 10 min, luminescence was detected with a SpectraMax Paradigm plate reader.

Fluor-de-Lys Assay. The reaction composition and conditions used were identical to conditions used in the *FLucK529ac lysine deacetylase assay* with the luciferase replaced by 10 μM Fluor-de-Lys peptide (Ac-Gly-Gly-Lys(ac)-AMC). All inhibitors were used at a concentration of 1 μM. The reaction was stopped by addition of an equal volume of 2× trypsin solution (0.1 mg/mL trypsin in sirtuin buffer 2). The fluorescence of the liberated coumarin (ex. 355 nm, em. 460 nm) was quantified after 5 min at RT using a FluoStar Omega Microplate Reader (BMG Labtech).

SirT-Glo Assay. Compounds were dispensed with the highest assay concentration of 10 μM in eight dilution steps and a factor of 3 into dry white 384-well plates (Corning 4513). Eight microliters of 15 nM SirT1 in 25 mM Tris/HCl pH 8.0, 137 mM NaCl, 2.7 mM KCl, 1 mM $MgCl_2$, 1 mM GSH, and 1 mM NAD^+ were added and incubated for 45 min at RT. Eight microliters of Glo-buffer with substrate and developer were added according to the manufacturer's protocol (Promega). After 10 min, luminescence was detected with a SpectraMax Paradigm plate reader.

ADP-Glo Control Assay (for Direct FLuc Inhibition). Compounds were dispensed as above. Eight microliters of kinase detection buffer with a substrate was added followed by incubation for 45 min at RT. Eight microliters of sirtuin buffer with 25 μM ADP and 1 mM NAD^+ was added, and after 10 min, luminescence was detected with a SpectraMax Paradigm plate reader.

Histone Deacetylation Assay. The deacetylation reactions were set up on ice in a 30 μL volume of sirtuin buffer 2 containing 250 μg/mL acid extracted histones,[36] 100 nM SirT1, 1 mM NAD^+, and varying concentration of inhibitors (10 mM stock solutions in DMSO). The reaction mixture was incubated for 30 min at 30 °C, and the reaction was stopped by addition of 10 μL 4× SDS-sample buffer. Ten microliters of the deacylation reactions were separated on an 18% SDS-PAGE and transferred to a PVDF membrane, and histone acetylation was detected using pan-specific acetyl-lysine antibody (Pan-AcK, PTM Biolabs, #105, 5% BSA/TBST 1:2000).

SirT1 Inhibitor Screening. HTS was carried out using the compound library of the Compound Management and Screening Center of the Max Planck Society, including ca. 170,000 commercial and proprietary compounds. Primary screening was carried out in 1536 well format at 12.5 μM yielding 4760 primary hits with residual SirT1 activity below 50%. After filtering for compound purity, 2800 compounds were retested for SirT1 activity in FLucK529ac lysine deacetylase and luciferase assays in quadruplicate. Eight hundred forty-two compounds were confirmed for SirT1 activity (mean residual activity of <50%) while after filtering for luciferase inhibition 135 hits remained. After additional PAINS filtering and testing against redox-cycling behavior, 115 hits remained, which were selectively profiled for SirT1, 2, and 3 in dose-response mode.

Redox-Cycling Compound Method. To exclude compounds that inactivate SirT1 through redox-cycling behavior, redox-cycling assays were carried out according to Tarnowski et al. with slight modifications.[30] Compounds were dispensed into dry black 384-well plates (Corning 4514). For the resazurin assay, 5 μM resazurin solution in 25 mM Tris/HCl pH 8.0, 137 mM NaCl, 2.7 mM KCl, 1 mM $MgCl_2$, 1 mM GSH, 3 μM DTT, and 1 mM NAD^+ was added. For the Amplex Ultrared assay, 25 μM Amplex Ultrared, 0.001 U/mL horseradish peroxidase, and 25 U/mL superoxide dismutase solution in 25 mM Tris/HCl pH 8.0, 137 mM NaCl, 2.7 mM KCl, 1 mM $MgCl_2$, 1 mM GSH, 3 μM DTT, and 1 mM NAD^+ were added. After 30 min, fluorescence was detected with a Paradigm Spectramax reader (EX535/EM595).

PAINS Filtering. The PAINS filtering was performed computationally according to Baell et al.,[29] and the structural features were taken in SMARTS encoding from Saubern et al.[37] In addition, structural features described by Dahlin et al.[38] were manually

https://doi.org/10.1021/acs.jmedchem.1c00017
J. Med. Chem. 2021, 64, 5838−5849

transformed into SMARTS and also removed. The PAINS filter was implemented as a Pipeline Pilot protocol that takes a list of compounds as input, filters out PAINS-containing structures by SMARTS-based substructure matching, and outputs only the PAINS-free compounds.

Chemical Synthesis and Characterization. An overview of the synthetic strategy of Sosbo compounds is shown in Schemes 1 and 2. Details on synthetic procedures and chemical characterization can be found in the Supporting Information. All test compounds were greater than 95% pure as determined using an Agilent 1100 Series HPLC equipped with a EC50/3 Nucleodur C18 Gravity column 1.8 μm from Macherey Nagel.

GloMelt Thermal Shift Assay. SirT1 or SirT3 (8 μM) was added into 384-well plates (LightCycler 480 Multiwell Plate 384, white) in buffer (25 mM Tris/HCl pH 8.0, 137 mM NaCl, 2.7 mM KCl, and 1 mM GSH) with 1 mM NAD^+ and 0.25 mM histone peptide H3K18ac as indicated. SirT2 (16 μM) was added into 384-well plates (Lightcycler 480,384-well plate, white) in buffer (25 mM Tris/HCl pH 8.0, 137 mM NaCl, 2.7 mM KCl, and 1 mM GSH) with 1 mM NAD^+ and 0.5 mM histone peptide H4K16ac as indicated. Selisistat (30 μM) or **4.27**/**4.3** (90 μM) was added followed by incubation for 20 min at RT. Upon addition of GloMelt dye (Biotium) into buffer (25 mM Tris/HCl pH 8.0, 137 mM NaCl, 2.7 mM KCl, and 1 mM GSH), thermal shift assays were run with a LightCycler 480 II (ROCHE) according to the manufacturer's protocol. Protein melting curves were analyzed, and ΔTm was calculated with LightCycler Thermal Shift Analysis software (ROCHE).

SYPRO Orange Thermal Shift Assay. All tested conditions were prepared in triplicate with each replicate containing 1 mg/mL purified SirT1, ± 1 mM NAD^+, ± 1 mM H3K18ac peptide (NH_2-GKAPRK[*Ac*]QLATK-COOH), ± 0.1 mM selisistat or **4.3**, and 10× SYPRO Orange in 20 μL sirtuin buffer 2. The change in fluorescence was measured in a rtPCR cycler using the following program: 20 °C 10 min, 360× [20 °C, 10 s, FRET Mode, +0.2 °C/Cycle], hold 8 °C. The experimental data were fitted with SciDavis (version 1.22) using a Boltzmann equation, determining the T_m of each replicate.

Treatment of MDA-MB-231 Cells with SirT1 Inhibitors and Western Blotting Analysis. MDA-MB-231 cells were grown in RPMI 1640 medium supplemented with GlutaMAX (Gibco), 10% FBS (Sigma-Aldrich), and 100 U/mL streptomycin−penicillin (Gibco). For treatment, 2 × 10^5 cells were seeded per well in a six-well plate containing 2 mL growth medium. The next day, 50 μM etoposide was added to induce p53 acetylation, and after 20 h, the medium was exchanged against 2 mL growth medium containing DMSO (2 μL), NAM (2 mM, in water), or inhibitor (1000× stock solution in DMSO). The medium was removed after 3 h, and the cells were washed with 1× PBS. The cells were lysed inside the wells by addition of 200 μL 231 lysis buffer (10 mM Tris−HCl pH 7.4, 150 mM NaCl, 15% glycerol, 1% Triton-X-100, 1× Pierce Protease Inhibitor Tablets (Thermo Scientific), and 0.05 mg/mL DNase I). The lysis was incubated for 20 min on ice. SDS was added to a concentration of 1% and incubated for another 10 min at room temperature while being agitated to solubilize all proteins. The lysate was collected and placed in a sonication bath for 10 min at RT to reduce its viscosity and then centrifuged for 10 min at 18,000 rpm. The supernatant (160 μL) was mixed with 40 μL 5× SDS-sample buffer, and 45 μL of each sample were separated on a 4−12% Bis-Tris NuPAGE Bolt gel (Novex). The immunoblot analysis was carried out using specific antibodies for p53 (AP6266b, abcepta, and 1:1000 in 3% BSA/PBS 0.1% Tween20), p53 K382Ac (#2525, Cell Signaling, 1:1000 in 5% BSA/TBS 0.1% Tween20), and H3 (ab1791, Abcam, 1:3000 in 3% BSA/TBS). The signal was developed using the antirabbit-HRP secondary antibody (A6154, Sigma-Aldrich, 1:10000 in 5% Milk/TBS) and ECL Select (GE Healthcare) western blotting detection agent.

Molecular Docking. Modeling, preparation, and visualization of structural data as well as molecular docking were performed using MOE 2019 software (Chemical Computing Group ULC, Canada). The crystal structure of SirT1 in complex with a selisistat analogue (PDB-ID 4I5I) was obtained from the RCSB Protein Data Bank and subjected to the Quickprep procedure of MOE 2019 including 3D-protonation for subsequent docking. The partial charges of all protein and ligand atoms were calculated using the implemented Amber14 force field. The docking site was defined by the surrounding amino acids and structural water molecules within a radius of 5 Å. Structural water molecules are characterized by limited mobility and therefore resolvable by X-ray crystallography, which is caused by at least two or three hydrogen bonds to adjacent amino acids and bound ligands. Cofactor NAD^+ is also included in the definition of the binding pocket because it is connected to the selisistat analogue inhibitor by conventional hydrogen bonds via structural water molecule 717 in the crystal structure of the SirT1 (PDB-ID 4I5I). Molecular docking was performed choosing the triangle matcher for placement of the ligand in the binding site and ranked with the London dG scoring function. The best 30 poses were passed to refinement and energy minimization in the pocket using the induced fit method, and the 10 best poses were rescored using the GBVI/WSA dG scoring function. Chimera from the University of California UCSF was used to calculate the RMSD value between crystallized and redocked SirT1 ligand (PDB-ID 4I5I).

■ ASSOCIATED CONTENT

Supporting Information

The Supporting Information is available free of charge at https://pubs.acs.org/doi/10.1021/acs.jmedchem.1c00017.

Full blots, replicate experiments, redocking of the selisistat analogue ligand, correlation of docking scores, overlay of docking poses, 2D interactions, docking poses of benzoxazine analogues, overlay of enantiomers, GBVI/WSA dG docking score, strains and plasmids, and detailed chemical procedures and characterization of compounds (PDF)

Table S1: Selectivity of initial hits toward SirT1 compared to SirT2 and SirT3 (XLSX)

Table S2: Orthogonal SirT-Glo assay results (XLSX)

Molecular formula strings (CSV)

An overview of Z′-factors for the high-throughput screen (XLSX)

Docking pose (PDB-Sosbo_4.2) (PDB)

Docking pose (PDB-Sosbo_4.3) (PDB)

Docking pose (PDB-Sosbo_4.6) (PDB)

Docking pose (PDB-Sosbo_4.7) (PDB)

Docking pose (PDB-Sosbo_4.8) (PDB)

Docking pose (PDB-Sosbo_4.10) (PDB)

Docking pose (PDB-Sosbo_4.16) (PDB)

Docking pose (PDB-Sosbo_4.21) (PDB)

Docking pose (PDB-Sosbo_4.22) (PDB)

Docking pose (PDB-Sosbo_4.23) (PDB)

Docking pose (PDB-Sosbo_4.27) (PDB)

■ AUTHOR INFORMATION

Corresponding Author

Heinz Neumann − *Department of Structural Biochemistry, Max Planck Institute of Molecular Physiology, Dortmund 44227, Germany; Department of Chemical Engineering and Biotechnology, University of Applied Sciences Darmstadt, Darmstadt 64295, Germany;* orcid.org/0000-0001-9657-1913; Phone: +496151.16-38203; Email: heinz.neumann@h-da.de

Authors

Martin Spinck − *Department of Structural Biochemistry, Max Planck Institute of Molecular Physiology, Dortmund 44227, Germany*

Matthias Bischoff − *Compound Management and Screening Center, Dortmund, Dortmund 44227, Germany*
Philipp Lampe − *Compound Management and Screening Center, Dortmund, Dortmund 44227, Germany*
Franz-Josef Meyer-Almes − *Department of Chemical Engineering and Biotechnology, University of Applied Sciences Darmstadt, Darmstadt 64295, Germany;* orcid.org/0000-0002-1001-3249
Sonja Sievers − *Compound Management and Screening Center, Dortmund, Dortmund 44227, Germany*

Complete contact information is available at: https://pubs.acs.org/10.1021/acs.jmedchem.1c00017

Author Contributions

[‖]M.S. and M.B. contributed equally.

Author Contributions

Conceptualization, H.N. and S.S.; methodology, M.S., M.B., and P.L., investigation, M.S., M.B., P.L., F.-J.M.-A., and H.N.; data curation, S.S.; writing − original draft, F.-J.M.-A. and H.N.; writing − review and editing, all authors; supervision, H.N. and S.S.; project administration, H.N. and S.S.; and funding acquisition, H.N.

Notes

The authors declare the following competing financial interest(s): Heinz Neumann and Martin Spinck hold a patent on the lysine deacetylase assay used in this manuscript.

■ ACKNOWLEDGMENTS

We thank Petra Geue for technical assistance and Sascha Gentz for peptide synthesis. This project was financially supported by the Behrens-Weise Foundation and the Max-Planck-Institute of Molecular Physiology.

■ ABBREVIATIONS

AMC, 7-amino-4-methylcoumarin; ATP, adenosine triphosphate; Boc, benzyloxycarbonyl; DCM, dichloromethane; DIPEA, N,N-Diisopropylethylamine; DMF, dimethylformamide; DMSO, dimethyl sulfoxide; DNAse, desoxyribonuclease; DTT, dithiothreitol; DTT, dithiothreitol; EDTA, ethylenediaminetetraacetic acid; EtOH, ethanol; FBS, fetal bovine serum; FLuc, Firefly Luciferase; FOXO, Forkhead box protein O; FRET, fluorescence resonance energy transfer; GSH, glutathione; H3K18ac, histone H3 K18 acetylation; H4K16ac, histone H4 K16 acetylation; HATU, 1-[Bis(dimethylamino)methylene]-1H-1,2,3-triazolo[4,5-*b*]pyridinium 3-oxide hexafluorophosphate; HTS, high-throughput screening; i.a., inter alia; IC_{50}, half-maximal inhibitory concentration; KDAC, lysine deacetylase; KM, Michaelis−Menten constant; NAD^+, nicotinamide adenine dinucleotide; NAM, nicotinamide; NTA, nitrilotriacetic acid; OAADPR, *O*-acetyl-ADP-ribose; PAINS, pan-assay interference compounds; PBS, phosphate buffered saline; PGC1-α, eroxisome proliferator-activated receptor gamma coactivator 1-alpha; PKA, protein kinase A; PMSF, phenylmethylsulfonyl fluoride; PVDF, polyvinylidene difluoride; RMSD, root mean square deviation; RT, room temperature; rtPCR, real-time polymerase chain reaction; SAR, structure−activity relationship; SDS-PAGE, sodium dodecyl sulfate polyacrylamide gel electrophoresisv; Sosbo, sirtuin one selective benzoxazine; STAC, sirtuin-activating compound; THF, tetrahydrofuran; Tris, tris(hydroxymethyl)aminomethane; Vmax, maximum enzymatic rate

■ REFERENCES

(1) Imai, S. I.; Guarente, L. NAD+ and sirtuins in aging and disease. *Trends Cell Biol.* **2014**, *24*, 464−471.
(2) Blum, C. A.; Ellis, J. L.; Loh, C.; Ng, P. Y.; Perni, R. B.; Stein, R. L. Sirt1 modulation as a novel approach to the treatment of diseases of aging. *J. Med. Chem.* **2011**, *54*, 417−432.
(3) Cantó, C.; Auwerx, J. Caloric restriction, SIRT1 and longevity. *Trends Endocrinol. Metab.* **2009**, *20*, 325−331.
(4) Vaquero, A.; Scher, M.; Lee, D.; Erdjument-Bromage, H.; Tempst, P.; Reinberg, D. Human SirT1 interacts with histone H1 and promotes formation of facultative heterochromatin. *Mol. Cell* **2004**, *16*, 93−105.
(5) Nemoto, S.; Fergusson, M. M.; Finkel, T. SIRT1 functionally interacts with the metabolic regulator and transcriptional coactivator PGC-1α. *J. Biol. Chem.* **2005**, *280*, 16456−16460.
(6) Rodgers, J. T.; Lerin, C.; Haas, W.; Gygi, S. P.; Spiegelman, B. M.; Puigserver, P. Nutrient control of glucose homeostasis through a complex of PGC-1α and SIRT1. *Nature* **2005**, *434*, 113−118.
(7) Brunet, A.; Sweeney, L. B.; Sturgill, J. F.; Chua, K. F.; Greer, P. L.; Lin, Y.; Tran, H.; Ross, S. E.; Mostoslavsy, R.; Cohen, H. Y.; Hu, L. S.; Cheng, H. L.; Jedrychowski, M. P.; Gygi, S. P.; Sinclair, D. A.; Alt, F. W.; Greenberg, M. E. Stress-Dependent Regulation of FOXO Transcription Factors by the SIRT1 Deacetylase. *Science* **2004**, *303*, 2011−2015.
(8) Motta, M. C.; Divecha, N.; Lemieux, M.; Kamel, C.; Chen, D.; Gu, W.; Bultsma, Y.; McBurney, M.; Guarente, L. Mammalian SIRT1 represses Forkhead transcription factors. *Cell* **2004**, *116*, 551−563.
(9) Luo, J.; Nikolaev, A. Y.; Imai, S. I.; Chen, D.; Su, F.; Shiloh, A.; Guarente, L.; Gu, W. Negative control of p53 by Sir2α promotes cell survival under stress. *Cell* **2001**, *107*, 137−148.
(10) Vaziri, H.; Dessain, S. K.; Eaton, E. N.; Imai, S.-I.; Frye, R. A.; Pandita, T. K.; Guarente, L.; Weinberg, R. A. HSIR2 SIRT1 functions as an NAD-dependent p53 deacetylase. *Cell* **2001**, *107*, 149−159.
(11) Cantó, C.; Gerhart-Hines, Z.; Feige, J. N.; Lagouge, M.; Noriega, L.; Milne, J. C.; Elliott, P. J.; Puigserver, P.; Auwerx, J. AMPK regulates energy expenditure by modulating NAD+ metabolism and SIRT1 activity. *Nature* **2009**, *458*, 1056−1060.
(12) Revollo, J. R.; Grimm, A. A.; Imai, S. I. The NAD biosynthesis pathway mediated by nicotinamide phosphoribosyltransferase regulates Sir2 activity in mammalian cells. *J. Biol. Chem.* **2004**, *279*, 50754−50763.
(13) Fulco, M.; Cen, Y.; Zhao, P.; Hoffman, E. P.; McBurney, M. W.; Sauve, A. A.; Sartorelli, V. Glucose restriction inhibits skeletal myoblast differentiation by activating SIRT1 through AMPK-mediated regulation of Nampt. *Dev. Cell* **2008**, *14*, 661−673.
(14) Gerhart-Hines, Z.; Dominy, J. E.; Blättler, S. M.; Jedrychowski, M. P.; Banks, A. S.; Lim, J. H.; Chim, H.; Gygi, S. P.; Puigserver, P. The cAMP/PKA pathway rapidly activates SIRT1 to promote fatty acid oxidation independently of changes in NAD+. *Mol. Cell* **2011**, *44*, 851−863.
(15) Borra, M. T.; O'Neill, F. J.; Jackson, M. D.; Marshall, B.; Verdin, E.; Foltz, K. R.; Denu, J. M. Conserved enzymatic production and biological effect of O-acetyl-ADP-ribose by silent information regulator 2-like NAD+-dependent deacetylases. *J. Biol. Chem.* **2002**, *277*, 12632−12641.
(16) Zhao, K.; Harshaw, R.; Chai, X.; Marmorstein, R. Structural basis for nicotinamide cleavage and ADP-ribose transfer by NAD +-dependent Sir2 histone/protein deacetylases. *Proc. Natl. Acad. Sci. U. S. A.* **2004**, *101*, 8563−8568.
(17) Tanner, K. G.; Landry, J.; Sternglanz, R.; Denu, J. M. Silent information regulator 2 family of NAD-dependent histone/protein deacetylases generates a unique product, 1-O-acetyl-ADP-ribose. *Proc. Natl. Acad. Sci. U. S. A.* **2000**, *97*, 14178−14182.
(18) Sauve, A. A.; Schramm, V. L. Sir2 regulation by nicotinamide results from switching between base exchange and deacetylation chemistry. *Biochemistry* **2003**, *42*, 9249−9256.
(19) Tissenbaum, H. A.; Guarente, L. Increased dosage of a sir-2 gene extends lifespan in Caenorhabditis elegans. *Nature* **2001**, *410*, 227−230.

(20) Kaeberlein, M.; McVey, M.; Guarente, L. The SIR2/3/4 complex and SIR2 alone promote longevity in Saccharomyces cerevisiae by two different mechanisms. *Genes Dev.* **1999**, *13*, 2570−2580.
(21) Rogina, B.; Helfand, S. L. Sir2 mediates longevity in the fly through a pathway related to calorie restriction. *Proc. Natl. Acad. Sci. U. S. A.* **2004**, *101*, 15998−16003.
(22) Napper, A. D.; Hixon, J.; McDonagh, T.; Keavey, K.; Pons, J. F.; Barker, J.; Yau, W. T.; Amouzegh, P.; Flegg, A.; Hamelin, E.; Thomas, R. J.; Kates, M.; Jones, S.; Navia, M. A.; Saunders, J. O.; DiStefano, P. S.; Curtis, R. Discovery of indoles as potent and selective inhibitors of the deacetylase SIRT1. *J. Med. Chem.* **2005**, *48*, 8045−8054.
(23) Robinette, T. M.; Nicholatos, J. W.; Francisco, A. B.; Brooks, K. E.; Diao, R. Y.; Sorbi, S.; Ricca, V.; Nacmias, B.; Brieño-Enríquez, M. A.; Libert, S. SIRT1 accelerates the progression of activity-based anorexia. *Nat. Commun.* **2020**, *11*, 1−10.
(24) Broussy, S.; Laaroussi, H.; Vidal, M. Biochemical mechanism and biological effects of the inhibition of silent information regulator 1 (SIRT1) by EX-527 (SEN0014196 or selisistat). *J. Enzyme Inhib. Med. Chem.* **2020**, *35*, 1124−1136.
(25) Ekblad, T.; Schüler, H. Sirtuins are unaffected by PARP inhibitors containing planar nicotinamide bioisosteres. *Chem. Biol. Drug Des.* **2016**, *87*, 478−482.
(26) Peck, B.; Chen, C. Y.; Ho, K. K.; Di Fruscia, P.; Myatt, S. S.; Charles Coombes, R.; Fuchter, M. J.; Hsiao, C. D.; Lam, E. W. F. SIRT inhibitors induce cell death and p53 acetylation through targeting both SIRT1 and SIRT2. *Mol. Cancer Ther.* **2010**, *9*, 844−855.
(27) Wössner, N.; Alhalabi, Z.; González, J.; Swyter, S.; Gan, J.; Schmidtkunz, K.; Zhang, L.; Vaquero, A.; Ovaa, H.; Einsle, O.; Sippl, W.; Jung, M. Sirtuin 1 inhibiting thiocyanates (S1th)—a new class of isotype selective inhibitors of NAD+ dependent lysine deacetylases. *Front. Oncol.* **2020**, *10*, 1−15.
(28) Spinck, M.; Ecke, M.; Sievers, S.; Neumann, H. Highly sensitive lysine deacetylase assay based on acetylated firefly luciferase. *Biochemistry* **2018**, *57*, 3552−3555.
(29) Baell, J. B.; Holloway, G. A. New substructure filters for removal of pan assay interference compounds (PAINS) from screening libraries and for their exclusion in bioassays. *J. Med. Chem.* **2010**, *53*, 2719−2740.
(30) Tarnowski, M.; Barozet, A.; Johansson, C.; Eriksson, P. O.; Engkvist, O.; Walsh, J.; Nissink, J. W. M. Utility of resazurin, horseradish peroxidase, and NMR assays to identify redox-related false-positive behavior in high-throughput screens. *Assay Drug Dev. Technol.* **2018**, *16*, 171−191.
(31) Bourlot, A. S.; Sánchez, I.; Dureng, G.; Guillaumet, G.; Massingham, R.; Monteil, A.; Winslow, E.; Pujol, M. D.; Mérour, J. Y. New substituted 1,4-benzoxazine derivatives with potential intracellular calcium activity. *J. Med. Chem.* **1998**, *41*, 3142−3158.
(32) Touzeau, F.; Arrault, A.; Guillaumet, G.; Scalbert, E.; Pfeiffer, B.; Rettori, M. C.; Renard, P.; Mérour, J. Y. Synthesis and biological evaluation of new 2-(4,5-dihydro-1H-imidazol-2-yl)-3,4-dihydro-2H-1,4-benzoxazine derivatives. *J. Med. Chem.* **2003**, *46*, 1962−1979.
(33) Solomon, J. M.; Pasupuleti, R.; Xu, L.; McDonagh, T.; Curtis, R.; DiStefano, P. S.; Huber, L. J. Inhibition of SIRT1 catalytic activity increases p53 acetylation but does not alter cell survival following DNA damage. *Mol. Cell. Biol.* **2006**, *26*, 28−38.
(34) Gertz, M.; Fischer, F.; Nguyen, G. T. T.; Lakshminarasimhan, M.; Schutkowski, M.; Weyand, M.; Steegborn, C. Ex-527 inhibits Sirtuins by exploiting their unique NAD+-dependent deacetylation mechanism. *Proc. Natl. Acad. Sci. U. S. A.* **2013**, *110*, E2772−E2781.
(35) Zhao, X.; Allison, D.; Condon, B.; Zhang, F.; Gheyi, T.; Zhang, A.; Ashok, S.; Russell, M.; MacEwan, I.; Qian, Y.; Jamison, J. A.; Luz, J. G. The 2.5 Å crystal structure of the SIRT1 catalytic domain bound to nicotinamide adenine dinucleotide (NAD+) and an indole (EX527 analogue) reveals a novel mechanism of histone deacetylase inhibition. *J. Med. Chem.* **2013**, *56*, 963−969.
(36) Spinck, M.; Neumann-Staubitz, P.; Ecke, M.; Gasper, R.; Neumann, H. Evolved, selective erasers of distinct lysine acylations. *Angew. Chem., Int. Ed.* **2020**, *59*, 11142−11149.
(37) Saubern, S.; Guha, R.; Baell, J. B. KNIME workflow to assess PAINS filters in SMARTS format. Comparison of RDKit and indigo cheminformatics libraries. *Mol Inf.* **2011**, *30*, 847−850.
(38) Dahlin, J. L.; Nissink, J. W. M.; Strasser, J. M.; Francis, S.; Higgins, L.; Zhou, H.; Zhang, Z.; Walters, M. A. PAINS in the assay: Chemical mechanisms of assay interference and promiscuous enzymatic inhibition observed during a sulfhydryl-scavenging HTS. *J. Med. Chem.* **2015**, *58*, 2091−2113.

https://doi.org/10.1021/acs.jmedchem.1c00017
J. Med. Chem. 2021, 64, 5838−5849